ARTICLE

CdSe Nanorods Dominate Photocurrent of Hybrid CdSe–P3HT Photovoltaic Cell

Martin Schierhorn,[†] Shannon W. Boettcher,[§] Jeffrey H. Peet,[‡] Elison Matioli,[‡] Guillermo C. Bazan,[†,‡] Galen D. Stucky,[†,‡] and Martin Moskovits[†,*]

[†]Department of Chemistry and Biochemistry and [‡]Department of Materials, University of California, Santa Barbara, California 93106, United States and [§]Department of Chemistry, University of Oregon, Eugene, Oregon 97403, United States

ABSTRACT Photovoltaic devices based on organic semiconductors require charge-separating networks (bulk heterojunctions) for optimal performance. Here we report on the fabrication of organic–inorganic photovoltaic devices with tailored (*n*-type) CdSe nanorod arrays aligned perpendicularly to the substrate. The nanorod lengths varied from 58 ± 12 to 721 ± 15 nm, while the diameters and inter-rod spacings were kept constant at 89.5 ± 7.5 and 41.3 ± 9.9 nm, respectively. Short-circuit densities improved linearly with nanorod length, resulting in power conversion efficiencies of up to 1.38% for cells with nanorods 612 ± 46 nm long. Notably, the cell's efficiency was dominated by exciton generation in the CdSe nanorods.

KEYWORDS: photovoltaic · organic · hybrid · nanorod · porous aluminum oxide

Photovoltaics based on organic semiconductors (OPVs) have grown in importance because of their tunable properties, ease of processability, and low cost. Because exciton diffusion lengths are generally low in such materials, it is essential to provide a charge-separating network throughout the photoactive layer (bulk heterojunction, BHJ) in order to optimize charge carrier collection. Traditionally, BHJs are created by blending electron-donor and -acceptor materials, which then spontaneously phase separate.[1] Often, the morphology of such BHJs is difficult to control, resulting in convoluted and incomplete transport pathways with consequential loss in power conversion efficiency.[2,3] One way of addressing these challenges is by substituting one of the organic phases with inorganic semiconductors (*e.g.*, CdSe,[4−8] CdS,[9,10] ZnO,[11−14] or TiO_2),[15−18] which exhibit higher mobilities, and whose dimensions and alignment can be more precisely controlled thereby ameliorating charge separation and the continuity of conduction pathways.[6,19,20] The morphology and shape of the inorganic phase are critically important as highlighted by Alivisatos and co-workers, who showed that by dispersing CdSe nanorods in place of quantum dots as the inorganic phase in a P3HT matrix, the efficiency of the devices could be improved dramatically.[5,6] Efficiencies up to 2.2% were recorded when using hyperbranched nanocrystals.[7]

We reason that a completely ordered system of straight nanorods all aligned perpendicular to the substrate could further improve charge carrier mobilities in the polymer because: (a) annealing could be carried out at higher temperatures without damaging the spatial distribution of organic/inorganic components,[12] and (b) the polymer chains tend to align within the interstitial spaces thereby potentially increasing charge carrier mobilities.[21] We have recently demonstrated the fabrication of inorganic semiconducting arrays with all nanorods aligned perpendicularly to a conducting transparent substrate using porous aluminum oxide (PAO) as a hard template.[22] Here, we exploit the benefits of this technique to investigate how incremental penetration of aligned CdSe nanorods into a poly(-3 hexylthiophene) (P3HT) matrix affects the photovoltaic device performance.

RESULTS AND DISCUSSION

CdSe nanorod arrays were deposited electrochemically onto ITO-coated glass through the channels of PAO. An intermediate 20 nm TiO_2 layer aided device fabrication and served as a hole-blocking layer in the final devices.[22,23] The interstitial spaces between the nanorods were infiltrated with P3HT, and the devices were completed with an Au top electrode (see Methods Section and Supporting Information.) A schematic of the final device along with an energy diagram is shown in Figure 1.

For the present study we fabricated devices with nanorod lengths varying from 58 ± 12 to 721 ± 15 nm while keeping the diameters and inter-rod spacings constant at

*Address correspondence to moskovits@chem.ucsb.edu.

Received for review July 23, 2010 and accepted September 17, 2010.

Published online September 28, 2010. 10.1021/nn101742c

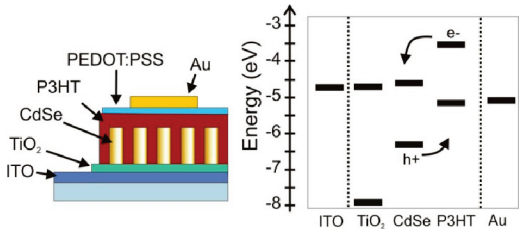

Figure 1. Schematic of a CdSe−P3HT hybrid photovoltaic device along with a corresponding energy diagram. The direction of flow of electrons and holes is also indicated.

89.5 ± 7.5 and 41.3 ± 9.9 nm, respectively (Figure 2). Typical current−voltage ($J-V$) curves are presented in Figure 3a. The values extracted from these curves are listed in Table 1 and plotted in Figure 3b−e. Devices without CdSe show negligible power conversion efficiencies ~0.01% (Figure 3e) and low short-circuit photocurrents (J_{SC} = 0.07 ± 0.02 mA cm^{-2}) (Figure 3b). The inclusion of CdSe nanorods with heights even as small as 58 ± 12 nm produces an order of magnitude increase in current density ~0.79 ± 0.31 mA cm^{-2} while maintaining the cell thickness constant at ~480 nm. Concurrently, the open-circuit voltage (V_{OC}) (Figure 3c) increases from 0.26 ± 0.01 to 0.44 ± 0.08 V and the fill factor (FF) (Figure 3d) increases from 0.37 ± 0.01 to 0.42 ± 0.02, augmenting the power conversion efficiency to 0.15 ± 0.07%. Continued increase in rod length leads to a linear increase in J_{SC} to a value of 4.79 ± 0.72 mA cm^{-2} for cells with 737 ± 15 nm rods. Over this range of rod-lengths, the V_{OC} (Figure 3c) varies between 0.4 and 0.6 V, while the FF (Figure 3d) remains approximately constant at ~0.45. Consequentially, the power conversion efficiency (η) also increases linearly with increasing nanorod length to 1.00 ± 0.14% for the longest rods fabricated. The best performing device was measured at 1.38% in power conversion efficiency under 100 mW cm^{-2} of AM 1.5G illumination.

The strong dependence of J_{SC} on the nanorod length can be rationalized by referring to the absorption characteristics (Figure 4). The absorptance of a substrate with only CdSe nanorods (Figure 4a, red circles) shows typical characteristics of CdSe with an onset occurring at ~730 nm.[24] The absorptance of P3HT (black squares) onsets at ~650 nm and peaks at 550 nm. The experimentally measured absorptance of the devices containing both CdSe nanorods and P3HT (green triangles) behaves very much like the linear combination of the two materials (see below). Hybrid devices with varying rod lengths do not show significant changes in the combined absorptance spectra for wavelengths smaller than the wavelength of peak P3HT absorption. However, for wavelengths between 730 and 550 nm—where only CdSe absorbs—the device's absorptance increases linearly with increasing nanorod length (Figure 4b). Overall, the device with longest nanorods absorbs only 26% more light than devices without CdSe, yet J_{SC} increases by almost two orders of magnitude. To understand this counterintuitive observation, we first considered the change in device performance on introducing the shortest CdSe nanorods, which produces an 11-fold increase in J_{SC}. Two factors can account for this enhancement: (a) The formation of a type-II heterojunction between CdSe and P3HT dramatically improves exciton separation and carrier collection as compared to what occurs for the bare TiO_2/P3HT system. The increase in V_{OC} is also consistent with this explanation, since the conduction band of TiO_2 is ~0.12 V lower than that of CdSe. (b) Light absorbed by the CdSe generates excitons in the inorganic phase, and since the exciton diffusion length is generally larger for inorganic than for organic semiconductors, these charges would be more effectively separated.

The observed linear increase in J_{SC} with increasing CdSe nanorod length is consistent with both of the above propositions. As the rods grow, the junction area between CdSe and P3HT also increases proportionately creating, thereby, a BHJ in which carrier collection from the polymer phase increases linearly with rod length.[25] At the same time, light absorption by the nanorods also increases, resulting in enhanced exciton generation in the inorganic phase. Below we show that it is, in fact, the increased light absorption by the CdSe that plays the major role.

A plot of the internal quantum efficiency (IQE) vs wavelength for a sample with ~610 nm long CdSe rods (Figure 5, blue triangles) clarifies the contribution of each material to the overall photocurrent. The device exhibits an IQE maximum of 95% at λ = 660 nm and a sharp decrease in IQE at λ = 525 nm, with values reaching a minimum of 29%. Referring to Figure 4a we see that the region with high IQE coincides with the spectral region where CdSe is the sole absorber, while the region where the efficiency drops significantly coincides with that of strong P3HT absorption.

This hitherto unreported behavior can be understood by first considering how exciton generation is distributed within the hybrid absorber layer.

The total absorptance, a_T, of the CdSe−P3HT hybrid cell is approximately given by

$$a_T = 1 - e^{-L(f_1\alpha_1 + f_2\alpha_2)} \quad (1)$$

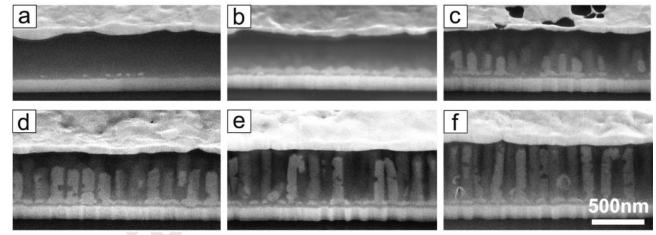

Figure 2. Cross-sectional SEM images of devices with different nanorod lengths: (a) no nanorods, (b) 58 ± 12, (c) 280 ± 85, (d) 368 ± 41, (e) 612 ± 46, and (f) 721 ± 15 nm. The images were taken at a tilt angle of 52°.

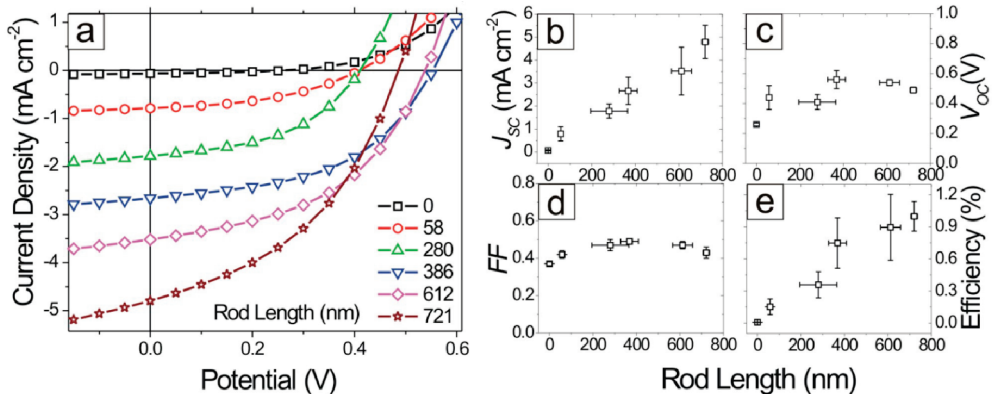

Figure 3. Current density vs voltage ($J-V$) measurements. (a) $J-V$ curves obtained from devices similar to those shown in Figure 2. The photovoltaic figures of merit extracted from these plots are shown as follows: (b) photogenerated short-circuit current density (J_{SC}), (c) open-circuit voltage (V_{OC}), (d) fill factor (FF), and (e) white light power conversion efficiency under 100 mW cm^{-2} of AM 1.5G illumination.

where f and α are the volume fractions and absorption coefficients of each absorber in the composite film, respectively, and L is the cell thickness. Using eq 1 we were able to reproduce the absorptance curve of the hybrid system from the absorptances of the individual components shown in Figure 4a (Supporting Information, Figure 2). The excellent match between the observed and computed absorptance spectrum of the composite indicates that, although heuristic, this is an appropriate approach. We acknowledge the fact that a composite material with structural elements smaller than the wavelength of light would behave optically like an effective optical medium whose optical constants could be predicted approximately by an effective medium theory, such as, for example, Bruggeman theory.[26] Using an absorptance spectrum for the nanopillars that is already that of a semiconductor/air effective medium goes a long way toward accounting for the nanostructure of the composite, as the goodness of correspondence between calculated and observed absorptance spectra indicates.

We estimate the relative fractions of the light, X_i, that are available to each of the absorbers as:

$$\frac{x_1}{x_2} = \frac{\alpha_1 f_1}{\alpha_2 f_2} \qquad (2)$$

where the sum of the fractions is unity. Knowing X_i, the IQE of the combined system can be predicted according to

where η_i is the efficiency of converting photons to useful electrons. From eq 3 it follows that if η of one material approaches zero, then the IQE is determined solely by the product ηX of the other material, and if we further assume the efficiency to be constant over the wavelengths considered, then the shape of the IQE curve should be entirely dictated by X. Traditional reasons for low efficiencies include: (a) the presence of a large barrier to charge injection from one material to the other, and/or (b) a very low exciton diffusion length preventing the photogenerated charges to reach the charge-separating junction. We calculated X_{CdSe} and X_{P3HT} by extracting the absorption coefficients from the data shown in Figure 4a (Supporting Information) and by using 42% as the CdSe volume fraction as determined from SEM. The fractions X_{CdSe} and X_{P3HT} are plotted along with IQE as a function of wavelength in Figure 5.

The striking similarity between the X_{CdSe} and the IQE suggests that most of the photocurrent is generated by the CdSe nanorods with very little or no contribution from the P3HT. Thus, the main reason for the observed linear increase in J_{SC} as a function of nanorod length is indeed the increased absorption by the CdSe, with negligible participation or collection improvement of the excitons formed in the P3HT. Effectively, the polymer acts solely as a highly efficient charge-separating, hole transporting layer (as evidenced by the high IQE in the red region of the spectrum), and CdSe is the sole

TABLE 1. Photovoltaic Figures of Merit As a Function of Nanorod Length and Cell Thickness[a]

rod length (nm)	cell thickness (nm)	J_{SC} (mA cm^{-2})	V_{OC} (V)	FF	η (%)
0	497 ± 29	0.07 ± 0.02	0.26 ± 0.01	0.37 ± 0.01	0.01 ± 0.00
58 ± 12	471 ± 21	0.79 ± 0.31	0.44 ± 0.08	0.42 ± 0.02	0.15 ± 0.07
280 ± 85	523 ± 41	1.78 ± 0.31	0.41 ± 0.05	0.47 ± 0.03	0.36 ± 0.12
368 ± 41	601 ± 16	2.66 ± 0.59	0.56 ± 0.06	0.49 ± 0.00	0.75 ± 0.24
612 ± 46	691 ± 41	3.52 ± 1.04	0.54 ± 0.02	0.47 ± 0.02	0.90 ± 0.31
721 ± 15	737 ± 15	4.79 ± 0.72	0.49 ± 0.02	0.43 ± 0.03	1.00 ± 0.14

[a]The cell thickness refers to the total thickness of the active layer, the symbols are as defined in the text with η representing the white light power conversion efficiency under 100 mW cm^{-2} of AM 1.5G illumination.

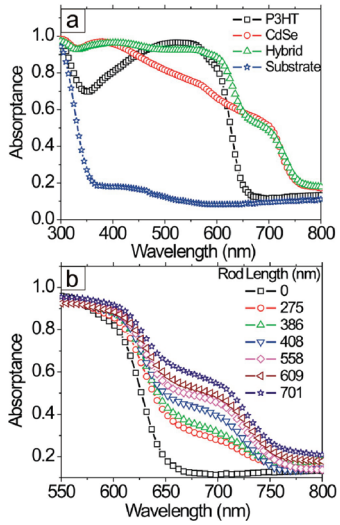

Figure 4. Absorption characteristics. (a) Measured absorptance of a 500 nm thick film of P3HT (black squares), a substrate containing nanorods of ~610 nm in length (red circles), a polymer−CdSe hybrid device with nanorods of ~610 nm in length (green triangles), and the background absorptance of a glass slide coated with ITO and TiO_2 (blue stars). (b) The increase in absorptance of hybrid devices as a function of nanorod length.

$$IQE = \eta_1 X_1 + \eta_2 X_2 \quad (3)$$

current generator. In fact, improved performance would be expected with a nonabsorbing charge-separating, hole-transporting material.

This result is unexpected since P3HT is commonly used as the photoactive component in organic solar cells. Previous reports on CdSe−P3HT hybrid systems

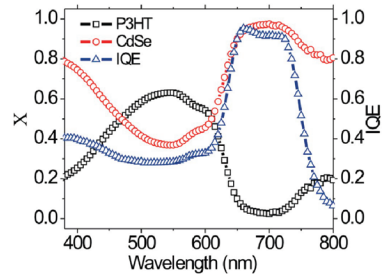

Figure 5. Comparison of the results from the optical model and the measured IQE. The calculated relative fractions of the light available (*X*) of P3HT (black squares) and the CdSe phase (red circles) compared with the measured IQE (blue triangles).

which employed CdSe nanostructures with smaller dimensions do not report an unusual IQE behavior, even though similar junctions between polymer and inorganic phase are expected.[6] We thus believe that the reason X_{P3HT} approaches zero is likely the low exciton diffusion length (typically ~3−10 nm) in the polymer.[27−29] Since the average distance between nanorods is 41 ± 10 nm, most of the excitons generated in the polymer would recombine before reaching the junction. Decreasing the distance between nanopillars should improve J_{SC} and thus the overall device performance. Alternatively, replacing the P3HT with a low-absorbance charge-separating, hole-transporting material should also result in a significant increase in cell efficiency and would be an intriguing strategy for fabricating high-efficiency nanostructured photovoltaics.

METHODS

Device Fabrication. The fabrication of CdSe nanorod arrays in the pores of PAO was described previously.[22] A detailed procedure is given in the Supporting Information. Briefly, ITO-coated glass was coated with 20 nm of TiO_2, followed by the deposition of 800 nm of Al, which was anodized in 0.3 M oxalic acid at 60 V. After pore widening in 5 wt % phosphoric acid for 65 min, CdSe was electrodeposited from an aqueous solution of $CdSO_4$ and SeO_2 in sulfuric acid by sweeping the voltage between −0.757 and −0.357 V vs Ag/AgCl at a rate of 0.75 V s^{-1}, which corresponds to a nanorod growth rate of 9.5 nm min^{-1}. Samples were annealed at 500 °C for 1 h in Ar, and the PAO was dissolved in NaOH. The nanorod surface was cleaned with 0.5% HF for 15 s. P3HT in chlorobenzene (30 mg/mL) was spun coated onto the substrates in a glovebox at 1100 rpm for 1 min. The samples were then heated at 230 °C for 1 h. Next, the P3HT surface was treated with an O_2 plasma at 650 mtorr and 35 mW for 10 s, followed by the application of a ~40 nm thick film of poly(3,4-ethylenedioxythiophene) poly(styrenesulfonate) (PEDOT:PSS) (Clevios 4083) spun at 2500 for 1 min. Au electrodes of 100 nm thickness were deposited in a thermal evaporator.

Optical Characterization. The absorptance was measured on a UV-Vis-NIR spectrometer (Shimadzu UV 3600) equiped with an integrating sphere (model ISR 3100). Solar power conversion efficiencies were determined in an inert atmosphere using a 330 W Oriel Xenon lamp with an AM 1.5 global filter. Solar simulator irradiance was set at 100 mW cm^{-2} using a Si photodiode with a KG5 optical filter calibrated at the National Renewable Energy Laboratory. External quantum efficiency (EQE) spectra measurements were made with a 75 W Xe source, a McPherson EU-700−56 monochromator, an optical chopper and lock-in amplifier, and a NIST traceable silicon photodiode for monochromatic power density calibration.

Acknowledgment. We gratefully acknowledge research support from the Institute for Energy Efficiency, an Energy Frontier Research Center funded by the United States Department of Energy, Office of Science, Office of Basic Energy Sciences, award number DE-SC0001009. This work made use of MRL Central Facilities supported by the MRSEC Program of the National Science Foundation under award no. DMR05-20415. A portion of the work was performed in the Univeristy Of California, Santa Barbara, Nanofabrication Facility, a part of the National Science Foundation funded National Nanofabrication Infrastructure Network (NNIN).

Supporting Information Available: Detailed experimental procedure. Explanation of optical model. EQE curve of hybrid device. This material is available free of charge *via* the Internet at http://pubs.acs.org.

REFERENCES AND NOTES

1. Yu, G.; Gao, J.; Hummelen, J. C.; Wudl, F.; Heeger, A. J. Polymer Photovoltaic Cells - Enhanced Efficiencies via a Network of Internal Donor-Acceptor Heterojunctions. *Science* **1995**, *270*, 1789–1791.
2. Peet, J.; Senatore, M. L.; Heeger, A. J.; Bazan, G. C. The Role of Processing in the Fabrication and Optimization of Plastic Solar Cells. *Adv. Mater.* **2009**, *21*, 1521–1527.

3. Nelson, J. Organic Photovoltaic Films. *Curr. Opin. Solid State Mater. Sci.* **2002**, *6*, 87–95.
4. Greenham, N. C.; Peng, X. G.; Alivisatos, A. P. Charge Separation and Transport in Conjugated-Polymer/Semiconductor-Nanocrystal Composites Studied by Photoluminescence Quenching and Photoconductivity. *Phys. Rev. B: Condens. Matter Mater. Phys.* **1996**, *54*, 17628–17637.
5. Huynh, W. U.; Dittmer, J. J.; Alivisatos, A. P. Hybrid Nanorod-Polymer Solar Cells. *Science* **2002**, *295*, 2425–2427.
6. Huynh, W. U.; Dittmer, J. J.; Teclemariam, N.; Milliron, D. J.; Alivisatos, A. P.; Barnham, K. W. J. Charge Transport in Hybrid Nanorod-Polymer Composite Photovoltaic Cells. *Phys. Rev. B: Condens. Matter Mater. Phys.* **2003**, *67*, 12.
7. Gur, I.; Fromer, N. A.; Chen, C. P.; Kanaras, A. G.; Alivisatos, A. P. Hybrid Solar Cells with Prescribed Nanoscale Morphologies Based on Hyperbranched Semiconductor Nanocrystals. *Nano Lett.* **2007**, *7*, 409–414.
8. Sun, B. Q.; Greenham, N. C. Improved Effciency of Photovoltaics Based on CdSe Nanorods and Poly(3-Hexylthiophene) Nanofibers. *Phys. Chem. Chem. Phys.* **2006**, *8*, 3557–3560.
9. Xi, D.; Zhang, H.; Furst, S.; Chen, B.; Pei, Q. Electrochemical Synthesis and Photovoltaic Property of Cadmium Sulfide-Polybithiophene Interdigitated Nanohybrid Thin Films. *J. Phys. Chem. C* **2008**, *112*, 19765–19769.
10. Lee, J.-C.; Lee, W.; Han, S.-H.; KimTae, G.; Sung, Y.-M. Synthesis of Hybrid Solar Cells Using CdS Nanowire Array Grown on Conductive Glass Substrates. *Electrochem. Commun.* **2009**, *11*, 231–234.
11. Beek, W. J. E.; Wienk, M. M.; Janssen, R. A. J. Hybrid Solar Cells from Regioregular Polytbiophene and ZnO Nanoparticles. *Adv. Funct. Mater.* **2006**, *16*, 1112–1116.
12. Greene, L. E.; Law, M.; Yuhas, B. D.; Yang, P. D. ZnO-TiO_2 Core-Shell Nanorod/P3HT Solar Cells. *J. Phys. Chem. C* **2007**, *111*, 18451–18456.
13. Peiro, A. M.; Ravirajan, P.; Govender, K.; Boyle, D. S.; O'Brien, P.; Bradley, D. D. C.; Nelson, J.; Durrant, J. R. Hybrid Polymer/Metal Oxide Solar Cells Based on ZnO Columnar Structures. *J. Mater. Chem.* **2006**, *16*, 2088–2096.
14. Olson, D. C.; Lee, Y. J.; White, M. S.; Kopidakis, N.; Shaheen, S. E.; Ginley, D. S.; Voigt, J. A.; Hsu, J. W. P. Effect of Polymer Processing on the Performance of Poly(3-Hexylthiophene)/ZnO Nanorod Photovoltaic Devices. *J. Phys. Chem. C* **2007**, *111*, 16640–16645.
15. Kwong, C. Y.; Choy, W. C. H.; Djurisic, A. B.; Chui, P. C.; Cheng, K. W.; Chan, W. K. Poly(3-Hexylthiophene): TiO_2 Nanocomposites for Solar Cell Applications. *Nanotechnology* **2004**, *15*, 1156–1161.
16. Zeng, T. W.; Lin, Y. Y.; Lo, H. H.; Chen, C. W.; Chen, C. H.; Liou, S. C.; Huang, H. Y.; Su, W. F. A Large Interconnecting Network within Hybrid MEH-PPV/TiO_2 Nanorod Photovoltaic Devices. *Nanotechnology* **2006**, *17*, 5387–5392.
17. Kim, S. S.; Jo, J.; Chun, C.; Hong, J. C.; Kim, D. Y. Hybrid Solar Cells with Ordered TiO_2 Nanostructures and MEH-PPV. *J. Photochem. Photobiol., A* **2007**, *188*, 364–370.
18. Mor, G. K.; Shankar, K.; Paulose, M.; Varghese, O. K.; Grimes, C. A. High Efficiency Double Heterojunction Polymer Photovoltaic Cells Using Highly Ordered TiO_2 Nanotube Arrays. *Appl. Phys. Lett.* **2007**, *91*, 152111.
19. Kannan, B.; Castelino, K.; Majumdar, A. Design of Nanostructured Heterojunction Polymer Photovoltaic Devices. *Nano Lett.* **2003**, *3*, 1729–1733.
20. Coakley, K. M.; McGehee, M. D. Conjugated Polymer Photovoltaic Cells. *Chem. Mater.* **2004**, *16*, 4533–4542.
21. Coakley, K. M.; Srinivasan, B. S.; Ziebarth, J. M.; Goh, C.; Liu, Y. X.; McGehee, M. D. Enhanced Hole Mobility in Regioregular Polythiophene Infiltrated in Straight Nanopores. *Adv. Funct. Mater.* **2005**, *15*, 1927–1932.
22. Schierhorn, M.; Boettcher, S. W.; Kraemer, S.; Stucky, G. D.; Moskovits, M. Photoelectrochemical Performance of CdSe Nanorod Arrays Grown on a Transparent Conducting Substrate. *Nano Lett.* **2009**, *9*, 3262–3267.
23. Schierhorn, M.; Boettcher, S. W.; Ivanovskaya, A.; Norvell, E.; Sherman, J. B.; Stucky, G. D.; Moskovits, M. Fabrication and Electrochemical Photovoltaic Response of CdSe Nanorod Arrays. *J. Phys. Chem. C* **2008**, *112*, 8516–8520.
24. Ninomiya, S.; Adachi, S. Optical Properties of Cubic and Hexagonal CdSe. *J. Appl. Phys.* **1995**, *78*, 4681–4689.
25. Fan, Z.; Razavi, H.; Do, J.-w.; Moriwaki, A.; Ergen, O.; Chueh, Y.-L.; Leu, P. W.; Ho, J. C.; Takahashi, T.; Reichertz, L. A.; Neale, S.; Yu, K.; Wu, M.; Ager, J. W.; Javey, A. Three-Dimensional Nanopillar-Array Photovoltaics on Low-Cost and Flexible Substrates. *Nat. Mater.* **2009**, *8*, 648–653.
26. Granvist, C. G.; Hunderi, O. Retardation Effects on the Optical Properties of Ultrafine Particles. *s. Rev. B: Solid State* **1977**, *16*, 1353–1358.
27. Mayer, A. C.; Scully, S. R.; Hardin, B. E.; Rowell, M. W.; McGehee, M. D. Polymer-Based Solar Cells. *Mater. Today* **2007**, *11*, 28–33.
28. Scully, S. R.; McGehee, M. D. Effects of Optical Interference and Energy Transfer on Exciton Diffusion Length Measurements in Organic Semiconductors. *J. Appl. Phys.* **2006**, *100*, 034907.
29. Shaw, P. E.; Ruseckas, A.; Samuel, I. D. W. Exciton Diffusion Measurements in Poly(3-Hexylthiophene). *Adv. Mater.* **2008**, *20*, 3516–3520.